JOURNAL OF Materials CHEMISTRY

The magnetic structure and properties of rhombohedral $Li_3Fe_2(PO_4)_3$

Anna S. Andersson,[a] Beata Kalska,[d] Petra Jönsson,[c] Lennart Häggström,[b] Per Nordblad,[c] Roland Tellgren[a] and John O. Thomas*[a]

[a]*Inorganic Chemistry, Ångström Laboratory, Uppsala University, Box 538, SE-751 21 Uppsala, Sweden. E-mail: josh.thomas@kemi.uu.se*
[b]*Department of Physics, Ångström Laboratory, Uppsala University, Box 530, SE-751 21 Uppsala, Sweden*
[c]*Department of Materials Science, Ångström Laboratory, Uppsala University, Box 534, SE-751 21 Uppsala, Sweden*
[d]*The Soltan Institute for Nuclear Studies, 05-400, Poland*

Received 20th March 2000, Accepted 2nd August 2000
First published as an Advance Article on the web 19th September 2000

Magnetic susceptibility measurements indicate that rhombohedral $Li_3Fe_2(PO_4)_3$, obtained by ion exchange of monoclinic $Na_3Fe_2(PO_4)_3$, exhibits a paramagnetic to antiferromagnetic transition at $T_N \approx 27$ K. Curie–Weiss-like behaviour is observed above this temperature, with an effective magnetic moment on the Fe^{3+} ions of 5.94 μ_B. A small spontaneous magnetic moment indicates weak ferrimagnetic behaviour. Mössbauer spectroscopy confirms the magnetic ordering; the narrow doublet at room temperature splits into sextets below 28 K. The transition to a magnetically ordered state is very sharp with only a narrow temperature region (29–28 K) of coexisting magnetic and non-magnetic regions. The values for the electric quadrupolar splitting indicate an angle of $\approx 56°$ between the principal *c*-axis and the magnetic field vector. The saturation magnetic hyperfine field of 54 T is representative of an Fe^{3+} ion in high-spin configuration. The neutron powder diffraction pattern exhibits extra magnetic peaks at 10 K, all indexable within the crystallographic unit cell. This suggests a model in which the iron atoms within any given sheet perpendicular to the *c*-axis are ferromagnetically aligned, but coupled antiferromagnetically to adjacent Fe sheets. The refined magnetic moment on the Fe atoms is 4.2 μ_B lying in the *ab* plane. A slightly better fit was obtained for a small net moment (0.7 μ_B) in the *c*-direction, which would explain the weak ferrimagnetism observed in the susceptibility measurements, but not the direction of the magnetic vector deduced from Mössbauer measurements.

Introduction

On the basis of its favourable redox properties, good ionic conductivity, and low cost, rhombohedral $Li_3Fe_2(PO_4)_3$ (NASICON-type compound) is seen as a potential insertion-electrode material in lithium–polymer batteries.[1] The compound is obtained by ion exchange from solid-state synthesized $Na_3Fe_2(PO_4)_3$.[1,2]

$Na_3Fe_2(PO_4)_3$ has monoclinic symmetry (space group: *C*2/*c*) with the cell parameters $a = 15.127(3)$, $b = 8.722(2)$ and $c = 8.793(1)$ Å, $\beta = 125.14(1)°$ at room temperature (denoted the α-phase).[2] The framework structure consists of FeO_6 octahedra and PO_4 tetrahedra linked through common corners. Within this framework, the sodium atoms can occupy three different sites. Small peaks are found in both X-ray single-crystal and powder data, which are not indexable within this cell; these can be attributed to a superstructure, related to the ordering of the sodium atoms.[2–4] The monoclinic subcell can also be described within the pseudo-hexagonal cell: $a' = b' = 8.731(2)$, $c' = 21.569(3)$ Å, $\gamma' = 120.07(2)°$.[2] $Na_3Fe_2(PO_4)_3$ exhibits two reversible polymorphic phase transitions: at 95 °C (α→β) and at 145 °C (β→γ), respectively.[2] The γ-phase has rhombohedral symmetry and can be described within the hexagonal cell: $a = 8.733(1)$ Å, $c = 21.798(2)$ Å. The relative occupancies of the three sodium sites differ for the three polymorphs.[2,3]

Magnetic susceptibility measurements of $Na_3Fe_2(PO_4)_3$ show a para- to antiferromagnetic transition at a Néel temperature (T_N) of 47 K[5–9] with a weak ferromagnetic contribution due to spin-canting.[5,9] The derived magnetic moments carried by the Fe^{3+} ions differ: 5.84 μ_B[6] and 5.2 μ_B.[9] In the magnetically ordered state, the Mössbauer spectrum of $Na_3Fe_2(PO_4)_3$ comprises a slightly asymmetric sextet, especially in the 30–40 K region below the transition temperature; this has been attributed to the two Fe sites.[7] The magnetic (and nuclear) structure at 2 K has been refined from neutron powder diffraction data[8] within the monoclinic cell (space group: *C*2/*c*); the spins were found to lie in the *ab* plane *ca.* 29° from the *a*-axis direction; the total magnetic moment carried by the Fe^{3+} ions is 2.9 μ_B. A later study at 15 K, in which a rhombohedral symmetry was assumed (space group: $R\bar{3}c$), indicated an antiferromagnetic arrangement of Fe moments with $\mu_{Fe} = 4.5(2)$ μ_B aligned at 42(4)° to the hexagonal *c*-axis.[9]

$Li_3Fe_2(PO_4)_3$ adopts a rhombohedral symmetry ($R\bar{3}$), with cell parameters: $a = 8.310(2)$ and $c = 22.506(5)$ Å (hexagonal setting).[2] The crystal structure has recently been solved from neutron powder diffraction data;[4] the structure is isotypic with $Li_3In_2(PO_4)_3$[10] and very similar to γ-$Na_3Fe_2(PO_4)_3$,[4] the major difference being the occupation of the alkali-metal ion sites. The framework structure again consists of FeO_6 octahedra and PO_4 tetrahedra linked through common corners (Fig. 1). The iron atoms occupy two symmetry-independent 6c sites. The lithium atom occupies a single general crystallographic site (18f) and surrounds itself with four oxygens in a quite regular tetrahedron.

The rhombohedral phase is metastable and, if heated above 570 °C, turns into a monoclinic modification;[2] this phase remains stable upon cooling to room temperature. The

 DOI: 10.1039/b002218g

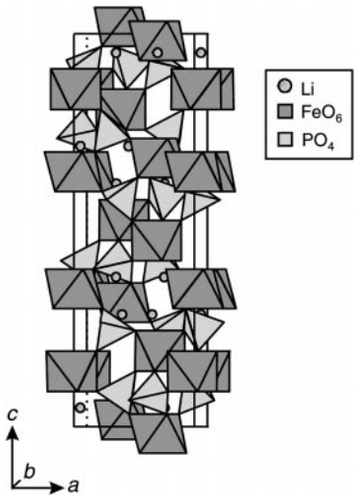

Fig. 1 The structure of rhombohedral $Li_3Fe_2(PO_4)_3$ viewed along the *b*-axis.

monoclinic phase can also be prepared by conventional solid-state synthesis; the cell parameters at room temperature (denoted the α-phase) are: $a=8.562(2)$, $b=12.005(3)$, $c=8.612(2)$ Å, $\gamma=90.51(2)^\circ$ (space group: $P2/n$).[11] Like the sodium compound, monoclinic $Li_3Fe_2(PO_4)_3$ exhibits several reversible phase transitions with temperature.[11] Very recently, magnetic susceptibility, electron spin resonance and Mössbauer results have been published for monoclinic $Li_3Fe_2(PO_4)_3$.[12] The compound orders antiferromagnetically below $T_N=29$ K. The two sextets in the Mössbauer spectra in the temperature region 19–23 K, with slightly different hyperfine parameters, indicate the two crystallographically independent Fe sites. The magnetic interaction in each Fe sublattice is ferromagnetic, but the two lattices are antiferromagnetically coupled.

To our knowledge, the magnetic properties of rhombohedral $Li_3Fe_2(PO_4)_3$ have not yet been investigated. In this paper, we present the results of magnetic susceptibility measurements, Mössbauer spectroscopy and neutron powder diffraction studies.

Experimental

The $Na_3Fe(PO_4)_3$ compound was synthesised according to two procedures.

Synthesis I

The sample used for the neutron diffraction studies was synthesised as follows: $Na_3Fe_2(PO_4)_3$ was prepared by the reaction of $NaH_2PO_4{\cdot}H_2O$, $Na_4P_2O_7{\cdot}10H_2O$ (≥99%, Merck) and Fe_2O_3 (≥99%, Merck) in the molar ratio 1 : 3.6 : 2.2.[2,4] The mixture was heated above the melting point (960 °C) for 5 h and cooled to room temperature for ~15 h. The resulting product was dissolved and thoroughly washed in water to remove excess sodium phosphates.

Synthesis II

The sample for the magnetic susceptibility measurements and for the Mössbauer spectroscopy study was synthesized as follows: $Na_3Fe_2(PO_4)_3$ was prepared by the solid-state reaction of $NaH_2PO_4{\cdot}H_2O$ (≥99%, Merck) and Fe_2O_3 (≥99%, Merck).[1] The synthesis was performed in consecutive steps; before each step, the material was ground and mixed thoroughly. The starting materials were first heated to 300 °C for a couple of hours, the temperature was then raised to 500 °C overnight to decompose the phosphate. The mixture was then heated to 920 °C for ~24 h. After grinding and homogenizing, the sample was pressed into pellets ($\phi=12$ mm, $P=3$ ton), annealed at 920 °C for another 24 h, and then allowed to cool slowly to room temperature. The last step was repeated to ensure the completeness of the reaction.

Rhombohedral $Li_3Fe_2(PO_4)_3$ was obtained by ion-exchanging the $Na_3Fe_2(PO_4)_3$ powder in a concentrated aqueous solution of $LiNO_3$ at slightly elevated temperature (35–40 °C), for at least 14 h. This ion exchange procedure was performed three times.

The phase purity of the synthesized material was checked by X-ray powder diffraction. The material prepared by Synthesis I contained very small amounts of some unidentified impurity. These few extra peaks were very small (relative intensities less than 1%) compared to the peaks from the majority phase.

Inductively Coupled Plasma atomic emission spectrometry (ICP) was used to determine the elemental composition of the synthesized material.

Magnetization and susceptibility measurements were performed on a Quantum Design MPMS 5.5T SQUID magnetometer. The zero-field-cooled (ZFC) magnetization was obtained by cooling the sample without an applied magnetic field, applying a field at the lowest temperature, and recording the magnetization as a function of temperature on heating. The field-cooled (FC) magnetization was measured during heating, having cooled the sample in the applied field.

Mössbauer spectroscopy measurements were carried out on a spectrometer with a constant-acceleration type vibrator with a 7 mCi ^{57}Co*Rh* source radiating in two opposite directions. The calibration spectra were recorded simultaneously at room temperature on one side, using natural iron foil as a reference absorber. Powder samples for low temperature studies were mixed with boron nitride and pressed into absorber discs. Low temperature spectra were recorded using a liquid-helium flow cryostat. The spectra obtained were folded and analysed using the commercial least-squares Mössbauer fitting program NORMOS.

The neutron diffraction measurements were performed at the R2 medium-flux steady-state research reactor in Studsvik, Sweden. A vanadium tube (9 mm in diameter) was filled with the powder sample and placed in a closed-cycle refrigerator cooled with helium. The data were collected with an array of 35 detectors, each separated by 4° in 2θ. A monochromatised neutron beam ($\lambda=1.470$ Å) was obtained with a double monochromator comprising two parallel copper crystals (Cu220).

Results

The ICP results for $Li_3Fe_2(PO_4)_3$ synthesized according to Syntheses I and II are shown in Table 1.

Magnetic susceptibility

The magnetic susceptibility curves plotted as a function of temperature at low magnetic fields for $Na_3Fe_2(PO_4)_3$ (NFP) and $Li_3Fe_2(PO_4)_3$ (R-LFP) are shown in Fig. 2. The corresponding inverse susceptibility curves are shown in Fig. 3. The magnetic behaviour of R-LFP is rather similar to that of NFP, both compounds exhibiting a phase transition at low temperature from paramagnetic to weakly ferrimagnetic. This transition occurs at a somewhat lower temperature for R-LFP ($T_N=27(1)$ K) than for NFP ($T_N=47(1)$ K). At temperatures above the transition temperature (100–300 K),

Table 1 Results of ICP analyses for rhombohedral $Li_3Fe_2(PO_4)_3$

	Molecular formula
Synthesis I	$Li_{2.93}Na_{0.04}Fe_{2.00}P_3O_{13.5}$
Synthesis II	$Li_{3.06}Na_{0.01}Fe_{2.16}P_3O_{12.2}$

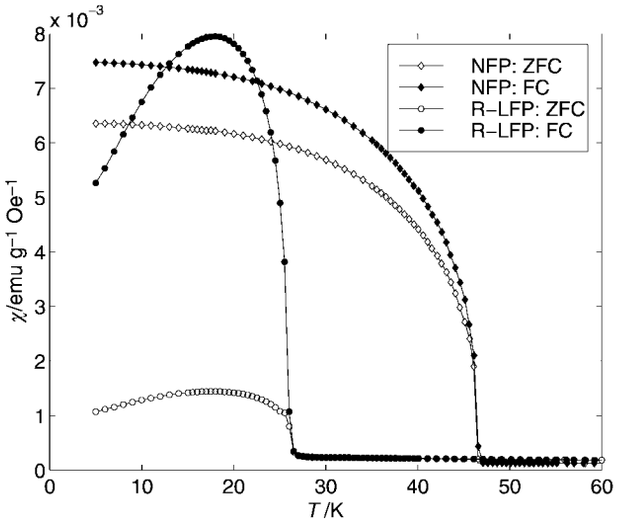

Fig. 2 Magnetic susceptibility curves as a function of temperature for monoclinic $Na_3Fe_2(PO_4)_3$ and rhombohedral $Li_3Fe_2(PO_4)_3$. Both zero-field cooled (ZFC) and field cooled (FC) curves are shown. The applied field (H) was 50 Oe (=5 mT).

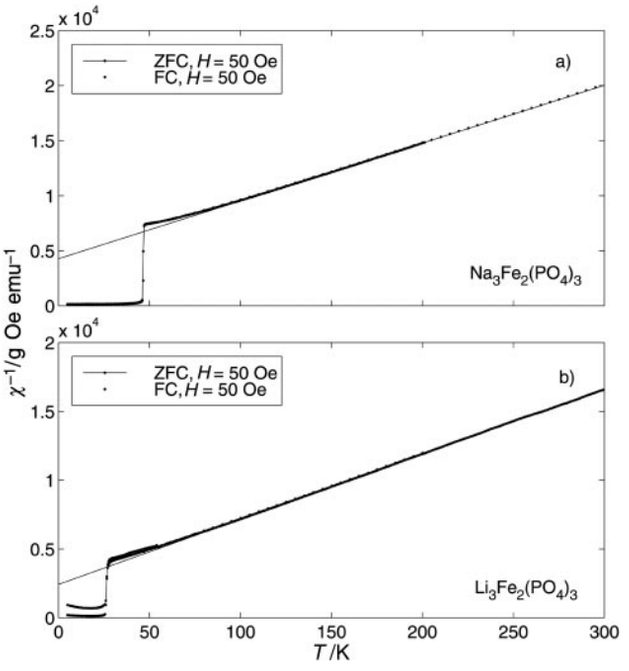

Fig. 3 The inverse magnetic susceptibility curves (ZFC and FC) as a function of temperature for (a) monoclinic $Na_3Fe_2(PO_4)_3$ and (b) rhombohedral $Li_3Fe_2(PO_4)_3$. $H=50$ Oe (=5 mT).

the susceptibility obeys the Curie–Weiss law for antiferromagnetic exchange: $\chi = C/(T+\theta_N)$, where $C=\mu_0 N m_{eff}^2/3k_B$ is the Curie constant and θ_N is the Weiss temperature. The effective magnetic moment, m_{eff}, carried by the Fe^{3+} ions derived from the Curie constant is 5.95(5) μ_B for NFP and 5.94(3) μ_B for R-LFP; the Weiss temperature is $\theta_N=-81(4)$ K for NFP and $\theta_N=-51(3)$ K for R-LFP (see Fig. 3). That the low-temperature phase is weakly ferrimagnetic can be seen from the difference between the ZFC and FC low-field susceptibilities, which is typical for ferrimagnetic materials. The magnetization *vs.* applied field (H) curve for R-LFP at 20 K is shown in Fig. 4. The spontaneous magnetic moment per Fe^{3+} ion is 0.027(5) μ_B at 20 K and 0.017(5) μ_B at 10 K for R-LFP (for NFP the spontaneous magnetic moment is 0.015(5) μ_B at 10 K).

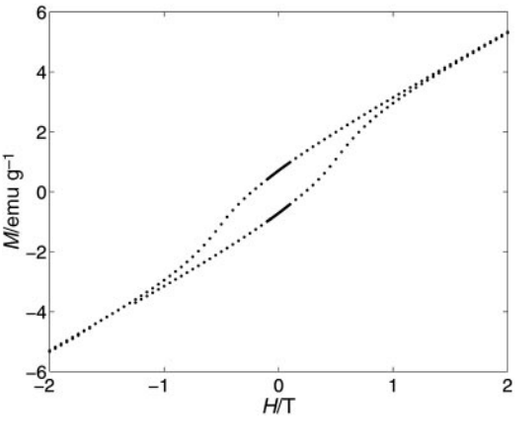

Fig. 4 Magnetization curves *vs.* the applied field (H) at 20 K for rhombohedral $Li_3Fe_2(PO_4)_3$.

Mössbauer spectroscopy

The room temperature spectrum can be fitted with a single doublet, isomer shift $\delta=0.46(1)$ mm s^{-1} (*vs.* natural α-Fe at 295 K) and electric quadrupole splitting $\Delta E_Q=0.18(1)$ mm s^{-1}. It should be noted, however, that a slightly better fit could be obtained if two doublets (according to the two different Fe sites) with almost equal centroid shifts, equal intensities, and slightly different quadrupole splittings were used in the fitting procedure (see Table 2). The rhombohedral compound becomes magnetically ordered at low temperature, with a transition temperature of 29(1) K (Fig. 5). This transition is very sharp with only a narrow temperature region of coexisting magnetic and non-magnetic regions, similar to the transition that NFP exhibits at $T_N=47$ K.[5,7] The hyperfine interaction parameters are presented in Table 2. Both Fe sites have a 3-fold rotational symmetry (about the c-axis), so that the principal z-

Table 2 Results from the fitting of the Mössbauer spectra for rhombohedral $Li_3Fe_2(PO_4)_3$ at low temperatures. The isomer shift, δ, (given *vs.* natural α-Fe at 295 K) is kept equal for all sub-spectra in the temperature range 16–28 K. Estimated errors on isomer shift, δ, electric quadrupole splitting, ΔE_Q, and absorber linewidth, w: ±0.01 mm s^{-1}; on magnetic hyperfine field, B: ±0.1 T; and on spectral intensity, I: ±2%. The bold row marks the temperature region in which both magnetic and non-magnetic components are observed

T/K	$\delta(1)$/mm s^{-1}	$\Delta E_Q(1)$/mm s^{-1}	$B_{hf}(1)$/T	$I(1)$ (%)	$\delta(2)$/mm s^{-1}	$\Delta E_Q(2)$/mm s^{-1}	$B_{hf}(2)$/T	$I(2)$ (%)	w/mm s^{-1}
295	0.45[a]	0.26	0	50[a]	0.45[a]	0.07	0	50[a]	0.12[b]
36	0.56	0.48	0	50	0.56	0.26	0	50	0.18[b]
30	0.56	0.47	0	50	0.56	0.28	0	50	0.22[b]
29	—	—	—	—	—	—	—	—	—
28	0.56[a]	−0.02	24.4	50[a]	0.56[a]	0.02	22.3	50[a]	0.10[b]
27	0.56[a]	−0.02	25.0	50[a]	0.56[a]	0.02	22.6	50[a]	0.11[b]
26	0.57[a]	−0.06	33.8	50[a]	0.57[a]	0.05	32.3	50[a]	0.12[b]
25	0.56[a]	−0.07	35.7	50[a]	0.56[a]	0.07	34.3	50[a]	0.12[b]
24	0.56[a]	−0.07	38.8	50[a]	0.56[a]	0.07	37.5	50[a]	0.11[b]
11	0.56[a]	−0.01	54.6	50[a]	0.56[a]	−0.02	53.7	50[a]	0.11[b]

[a]Values were constrained to be the same for both components. [b]Values were constrained to be the same for both components in *all* fittings.

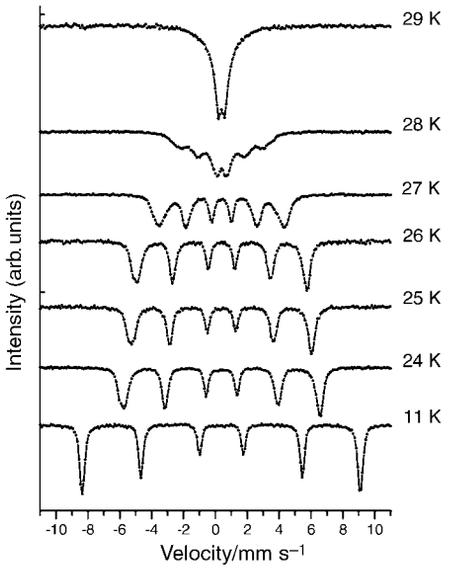

Fig. 5 Mössbauer spectra recorded between 11 K and 29 K for rhombohedral $Li_3Fe_2(PO_4)_3$.

axis of the electric field gradient (EFG) tensor is along this axis, and the asymmetry parameter (η) of the EFG is zero. This tells us that the paramagnetic electric quadrupole splitting (ΔE_Q) is $eQV_{zz}/2$, where V_{zz} is the principal component of the EFG. In first-order perturbation theory, the magnetic electric quadrupole splitting (ΔE_Q) is given by:

$$\Delta E_Q = \frac{eQV_{zz}}{2}\left(\frac{3\cos^2\theta - 1}{2}\right)$$

for $\eta = 0$. Using the values for ΔE_Q just above T_N and at 11 K (Table 2), we arrive at an angle $\theta \approx 56^\circ$ for the magnetic field vector with respect to the *c*-axis at 11 K (for both Fe atoms). The saturation magnetic hyperfine field of 54 T is representative for Fe^{3+} ions in high-spin configuration.

Neutron diffraction

The neutron powder diffractograms for R-LFP recorded at 295 K and 10 K are shown in Fig. 6. The small inset in Fig. 6(b) shows the difference between the observed intensities at 10 K and 30 K, *i.e.*, the purely magnetic part of the scattering. The diffraction data were refined using the Rietveld program FULLPROF,[13] where the crystal and magnetic structures are treated as a coupled two-phase system. The room-temperature data-set was first refined to check the structural parameters (starting parameters were those given by Masquelier *et al.*[4]). In all, 42 parameters were varied: 1 scale factor, the 2θ zero-point, 5 background coefficients, 2 cell parameters, 3 half-width parameters, 1 profile-shape parameter, 1 asymmetry parameter, 20 atomic coordinates and 8 isotropic temperature factors (one for each atom). The parameters thus obtained were used in the refinement of the 30 K data-set, and these parameters were, in turn, used for the refinement of the 10 K data-set. The temperature factors for the two Fe atoms were in this case constrained to be equal. A simple collinear antiferromagnetic model (Model A) was first assumed, with sheets of Fe atoms ferromagnetically aligned within the sheet, but antiferromagnetically coupled to adjacent sheets, *i.e.* all Fe(1) atoms have spins in one direction, and all Fe(2) atoms in the opposite direction. The absolute value of the magnetic moment was constrained to be the same for all Fe atoms. At an early stage in the refinement, it became clear that the M*x*/M*y* component was the largest contributor to the magnetic scattering. The moment found on the Fe atoms after refining

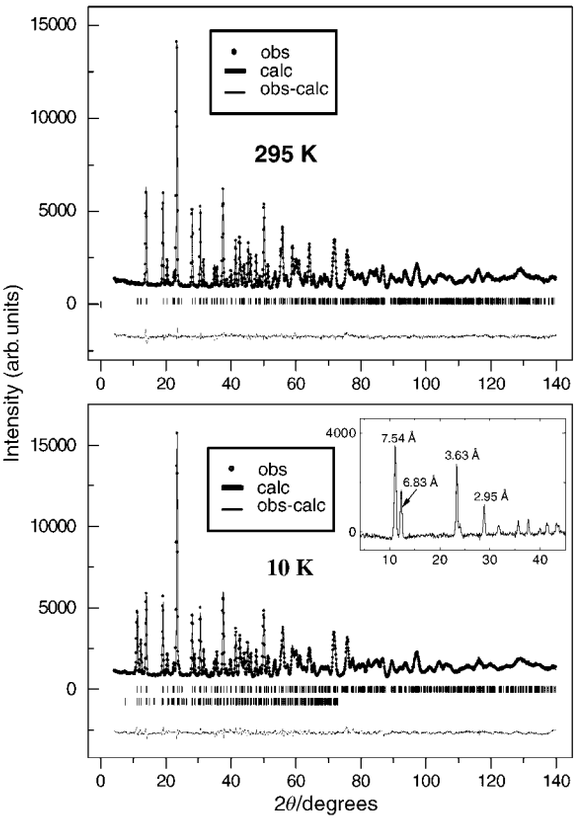

Fig. 6 Rietveld refinement fit for neutron diffraction profile of rhombohedral $Li_3Fe_2(PO_4)_3$ at (a) 295 K and (b) 10 K. The small inset in (b) shows the difference between the observed diffractograms at 10 K and 30 K, *i.e.*, the magnetic scattering contribution.

the M*x* component is: 4.19(4) μ_B in the *ab* plane. After refining all the structural parameters, the M*z* components were also refined, either with the same sign for Fe(1) and Fe(2) (Model A′) or with opposite signs (Model A″). Model A′ gave a slightly better fit (than Model A), with a magnetic moment of 0.7(2) μ_B in the *c*-direction on each atom, corresponding to a total moment of 4.25(5) on the Fe atoms, directed at an angle of $\sim 9^\circ$ out of the *ab* plane. The results from these refinements are given in Table 3, and the atomic coordinates obtained at 10 K in Table 4. It can be noted that a constrained refinement with an angle of 35° out of the *ab* plane (as suggested by the Mössbauer data) gave an *R* value of 13.9 for the magnetic phase, as compared to 3.5 for the unconstrained refinement. A comparison is made between some selected bond lengths obtained at room temperature and 10 K in Table 5.

Table 3 Overall parameters and Rietveld refinement agreement factors from neutron powder diffraction ($\lambda = 1.470$ Å) for rhombohedral $Li_3Fe_2(PO_4)_3$ at 295, 30 and 10 K. The listed reliability factors (except R_{Bragg}) are based on all non-excluded points, prior to background correction

	295 K	30 K	10 K
Space group	$R\bar{3}$	$R\bar{3}$	$R\bar{3}$
a/Å	8.3033(5)	8.2788(7)	8.2772(7)
c/Å	22.5232(14)	22.6319(22)	22.6313(20)
V/Å^3	1344.8 (2)	1343.3(3)	1342.8(2)
No. refined parameters	42	42	43
R_p (%)	3.1	3.9	4.0
R_{wp} (%)	4.1	5.0	5.2
R_{exp} (%)	2.6	2.6	2.6
χ^2	2.5	3.7	4.0
R_{Bragg} (%)	4.1	3.9	4.2
R_{magn} (%)	—	—	3.5

Table 4 Final atomic coordinates and isotropic temperature factors for rhombohedral $Li_3Fe_2(PO_4)_3$ at 10 K

Atom	Site	x	y	z	B_j/Å^2
Li	18f	0.355(4)	0.045(3)	0.382(1)	2.9(5)
Fe(1)	6c	0	0	0.1465(4)	0.15(6)[a]
Fe(2)	6c	0	0	0.6513(4)	0.15(6)[a]
P	18f	0.2902(9)	−0.0012(11)	0.2509(5)	0.6(1)
O(1)	18f	0.1898(8)	−0.0126(7)	0.1933(3)	0.4(1)
O(2)	18f	0.7677(8)	0.9079(8)	0.7005(3)	0.8(2)
O(3)	18f	0.2390(8)	−0.1981(7)	0.2680(3)	0.4(2)
O(4)	18f	0.4988(7)	0.8818(8)	0.7565(3)	0.2(2)

[a]Values constrained to be equal.

Table 5 Selected bond lengths (in Å) for rhombohedral $Li_3Fe_2(PO_4)_3$ at room temperature (RT) and 10 K

	RT[a]	RT	10 K
Li–O(2)	1.92(2)	1.98(2)	1.93(3)
O(2)	2.20(2)	2.28(2)	2.25(3)
O(3)	1.88(2)	1.94(2)	1.95(3)
O(4)	2.11(2)	1.94(2)	1.96(3)
⟨Li–O⟩	2.03	2.04	2.02
Fe(1)–O(1) ×3	1.929(6)	1.928(6)	1.940(7)
O(4) ×3	2.063(5)	2.065(6)	2.062(7)
⟨Fe(1)–O⟩	2.00	2.00	2.00
Fe(2)–O(2) ×3	1.996(5)	2.010(6)	2.014(7)
O(3) ×3	2.020(5)	1.989(5)	2.004(7)
⟨Fe(2)–O⟩	2.01	2.00	2.01
P–O(1)	1.555(7)	1.524(8)	1.522(10)
O(2)	1.524(6)	1.546(8)	1.552(10)
O(3)	1.548(5)	1.540(7)	1.515(9)
O(4)	1.505(6)	1.524(8)	1.526(8)
⟨P–O⟩	1.53	1.53	1.53

[a]Masquelier *et al.*[4]

Discussion

Structure *vs.* magnetic interaction

It would appear that the structures of NFP and R-LFP are similar enough to suggest that the effect of the ion exchange on the magnetic structure is small. However, the strength of the exchange interaction, J, between the Fe atoms is lowered going from NFP to R-LFP since J is proportional to T_N.

Also, both modifications of LFP show similar magnetic behaviour; *i.e.* both have a transition to a magnetically ordered state around 27–29 K. Both compounds exhibit a weak ferrimagnetic component according to the magnetic susceptibility measurements.

It is also interesting to note the similarity between the magnetic behaviour of LFP and $NaFeP_2O_7$.[14] Both are antiferromagnetic, with transition temperature around 29 K and similar Mössbauer parameters at both room and low temperatures.

The neutron diffraction data suggest that the Fe ion moments are oriented almost in the *ab* plane (the contribution in the *c*-direction must be small). All Fe atoms in a given sheet, perpendicular to the *c*-axis, are ferromagnetically aligned but coupled antiferromagnetically to adjacent Fe sheets (Fig. 7(a)). This model, with the spins lying mainly in the *ab* plane, agrees better with the results of Fanjat *et al.*[8] for NFP than with the results of the later study by Greaves *et al.*[9] Since the *a* and *b* axes are equivalent in the hexagonal setting, it is not possible to say anything about the spin direction within the *ab* plane from powder data. However, since both these structures are very similar (the major differences involve the occupation of alkalication sites), we can assume that the directions of the spins also coincide. In Fig. 7(b), the results from Fanjat *et al.*[8] for monoclinic NFP have been transferred to our hexagonal cell for R-LFP. If the directions of the spins on the Fe atoms are the same in both structures, this would mean that the spins lie parallel to the *a*-axis in R-LFP.

It would appear that the antiferromagnetic arrangement of spins is such that the magnetic unit cell is commensurate with the structural unit cell, and no superlattice peaks appear. This was also observed by Fanjat *et al.*[8]

The Mössbauer data suggest an angle of 30–35° for the magnetic vector with respect to the *ab* plane; this is not in agreement with the ND results. The reason for this significant discrepancy is unclear at this time. Some temperature dependence of the magnetic-spin orientation has been observed in several systems; however, the neutron diffraction and Mössbauer spectroscopy data were collected at the same temperature (10–11 K), which would exclude any such effect here.

The magnetic behaviour is probably also highly sensitive to the synthesis method used, the thermal history of the sample and the local ordering in the material. As for R-LFP, another factor must also be considered; namely, the degree of Li/Na exchange. Chemical analysis shows that the Na/Li molar ratio is less than 1 : 50, but even this small amount could well influence the effective local symmetry. It should be noted, however, that a neutron diffraction measurement made on a Synthesis II material at 10 K gave the same results (within two standard deviations) as a similar measurement on a Synthesis I material.

The observed effective magnetic moment, 5.94(3) μ_B, compares well with a high-spin state with a quenched orbital momentum for the Fe^{3+} ions, *i.e.* $J=5/2$ and $g_J=2$. Thus the Fe^{3+} magnetic moment, defined as $m=g_J\mu_B J$ would be 5.0 μ_B, a value higher than the moment found by neutron diffraction.

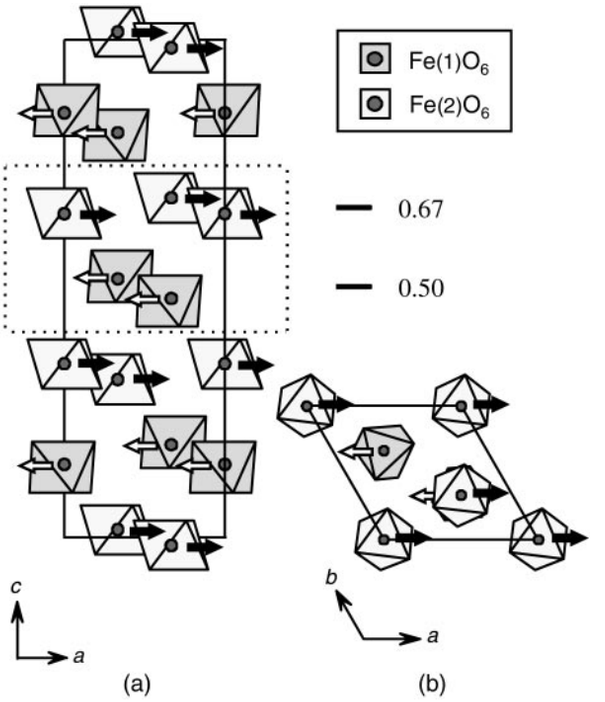

Fig. 7 The magnetic structure of rhombohedral $Li_3Fe_2(PO_4)_3$ (a) viewed along the *b*-axis and (b) viewed along the *c*-axis. The arrows symbolize the orientation of the Fe^{3+} magnetic moments in the cell. The white arrows pointing to the left are situated on Fe(1); the black arrows pointing to the right are situated on Fe(2). The area enclosed by the dotted rectangle in (a) contains the two layers (perpendicular to the *c*-axis) drawn in (b). The numbers given in the figure are the corresponding *z*-coordinates. *Note*: The directions of the magnetic moments in the *ab* plane are based on the assumption that the orientations of the spins within the *ab* plane are the same for monoclinic $Na_3Fe_2(PO_4)_3$ and rhombohedral $Li_3Fe_2(PO_4)_3$; the results from Fanjat *et al.*[8] have been transferred to a hexagonal cell.

As discussed in the Introduction, this material—along with other iron-containing compounds—is interesting as a lithium insertion material in battery applications. At present, the lithium insertion mechanism is unclear. Results so far indicate that the framework structure remains intact,[15,16] even though the insertion mechanism would seem to be more complex than was first believed. In earlier work, we have used *in situ* Mössbauer spectroscopy (among other techniques) to follow lithium insertion into R-LFP.[16] It remains unclear, however, where the extra lithium is inserted into the structure.

Interesting future work would therefore be to study the effect on the magnetic properties (transition temperature, magnetic ordering, *etc*.) of lithium insertion. There are examples in the literature where magnetic susceptibility and Mössbauer measurements (in magnetic states) have been used to characterize the compounds formed on lithium insertion, *e.g.* in spinel ferrites[17] and, more recently, in $Li_xV_6O_{13}$,[18] the spinel phase $Li_{1+x}Mn_{2-x}O_{4-\delta}$[19] and in the ordered rock-salt type structure $Li_{1-x}Ni_{1+x}O_2$.[19]

Acknowledgements

This work has been supported by grants from The Swedish Natural Science Research Council (NFR) and The Swedish Board for Technical Development (NUTEK). Håkan Rundlöf at the Neutron Research Laboratory (NFL), Studsvik, is also acknowledged for his skilled assistance in collecting the neutron diffraction data and Dominique Aernout for valuable help with Mössbauer spectroscopy measurements.

References

1 C. Masquelier, A. K. Padhi, K. S. Nanjundaswamy and J. B. Goodenough, *J. Solid State Chem.*, 1998, **135**, 228.
2 F. d'Yvoire, M. Pintard-Scrépel, E. Bretey and M. de la Rochère, *Solid State Ionics*, 1983, **9 & 10**, 851.
3 M. de la Rochère, F. d'Yvoire, G. Collin, R. Comès and J. P. Boilot, *Solid State Ionics*, 1983, **9 & 10**, 825.
4 C. Masquelier and J. Rodriguez-Carvajal, *Chem. Mater.*, 2000, **12**, 525.
5 D. Beltran-Porter, R. Olazcuaga. L. Fournes, F. Menil and G. Le Flem, *Rev. Phys. Appl.*, 1980, **15**, 1155.
6 D. Beltran-Porter, R. Olazcuaga. C. Delmas, F. Cherkaoui, R. Brochu and G. Le Flem, *Rev. Chim. Minéral.*, 1980, **17**, 458.
7 R. Salmon, R. Olazcuaga, Z. Jirak, D. Beltran-Porter, L. Fournes, F. Menil and G. Le Flem, *Solid State Chemistry, Proceedings of the 2nd European Conference,, 1982 Veldhoven, The Netherlands*, ed. R. Metselaar, H. J. M. Heijligers and J. Schoonman, Elsevier Science Publishers, Amsterdam, 1983.
8 N. Fanjat and J. L. Soubeyroux, *J. Magn. Magn. Mater.*, 1992, **104–107**, 933.
9 C. Greaves, P. R. Slater, M. Slaski and C. M. Muirhead, *Physica B*, 1994, **194–196**, 199.
10 E. A. Genkina, L. A. Muradyan, B. A. Maksimov, B. Merinov and S. E. Sigarev, *Sov. Phys. Crystallogr.*, 1987, **32**, 40.
11 A. B. Bykov, A. P. Chirkin, L. N. Demyanets, S. N. Doronin, E. A. Genkina, A. K. Ivano-Shitz, I. P. Kondratyuk, B. A. Maksimov, O. K. Mel'nikov, L. N. Muryadyan, V. I. Simonov and V. A. Timofeeva, *Solid State Ionics*, 1990, **38**, 31.
12 A. Goñi, L. Lezama, N. O. Moreno, L. Fournès, R. Olazcuaga, G. E. Barberis and T. Rojo, *Chem. Mater.*, 2000, **12**, 62.
13 J. Rodriguez-Carvajal, *Physica B*, 1993, **192**, 55.
14 R. C. Mercader, L. Terminiello, G. J. Long, D. G. Reichel, K. Dickhaus, R. Zysler, R. Sanchez and M. Tovar, *Phys. Rev. B*, 1990, **42**, 25.
15 C. Masquelier, J. Gaubicher and M. Quarton, *196th Electrochemical Soc. Meeting, Nov. 1999, Hawaii*, Abstract No. 220.
16 A. S. Andersson, B. Kalska, P. Eyob, L. Häggström and J. O. Thomas, *Solid State Ionics*, submitted.
17 C. J. Chen, M. Greenblatt and J. V. Waszczak, *Solid State Ionics*, 1986, **18&19**, 838.
18 C. Lampe-Önnerud, P. Nordblad and J. O. Thomas, *Solid State Ionics*, 1995, **81**, 189.
19 A. Ott, P. Endres, V. Klein, B. Fuchs, A. Jäger, H. A. Mayer, S. Kemmler-Sack, H.-W. Praas, K. Brandt, G. Filoti, V. Kunczer and M. Rosenberg, *J. Power Sources*, 1998, **72**, 1.